



ELSEVIER

ScienceDirect

Proceedings of the Combustion Institute xxx (2014) xxx–xxx

Proceedings
 of the
Combustion
Institute
www.elsevier.com/locate/proci

Nonlinear dynamics of a self-excited thermoacoustic system subjected to acoustic forcing

Saravanan Balusamy¹, Larry K.B. Li^{*,1}, Zhiyi Han, Matthew P. Juniper, Simone Hochgreb

Department of Engineering, University of Cambridge, Trumpington Street, Cambridge CB2 1PZ, UK

Abstract

We experimentally study the nonlinear dynamics of a self-excited thermoacoustic system subjected to acoustic forcing. Our aim is to relate these dynamics to the behavior of universal model oscillators subjected to external forcing.

The self-excited system under study consists of a swirl-stabilized turbulent premixed flame (equivalence ratio of 0.8 and thermal power of 13.6 kW) enclosed in a quartz tube with an open-ended exit. We acoustically force this system at different amplitudes and frequencies, and measure its response with pressure transducers and OH* chemiluminescence from the flame. By analyzing the data with the power spectral density and the Poincaré map, we find a range of nonlinear dynamics, including (i) a shifting of the self-excited frequency towards or away from the forcing frequency as the forcing amplitude increases; (ii) an accompanying transition from periodicity to two-frequency quasiperiodicity; and (iii) an eventual suppression of the self-excited amplitude, indicating synchronization of the self-excited mode with the forced mode. By further analyzing the data with the Hilbert transform, we find evidence of phase trapping, a partially synchronous state characterized by frequency locking without phase locking.

All of these dynamics can be found in universal model oscillators subjected to external forcing. This suggests that such oscillators can be used to accurately represent thermoacoustically self-excited combustion systems subjected to similar forcing. It also suggests that the analytical solutions to such oscillators can be used to guide the reduction and analysis of experimental or numerical data obtained from real thermoacoustic systems, and to identify effective methods for open-loop control of their dynamics.

© 2014 The Combustion Institute. Published by Elsevier Inc. All rights reserved.

Keywords: Thermoacoustics; Nonlinear dynamics; Combustion instability; Turbulent premixed flames; Low-order modeling

1. Introduction

Despite decades of research, thermoacoustic instability remains one of the biggest challenges

facing manufacturers of gas turbines. In these devices, the acoustics is usually linear,¹ but the flame's heat-release response to incident perturbations is highly nonlinear [1]. The overall thermoacoustic

* Corresponding author. Tel.: +44 7726 105674.

E-mail address: l.li@gatescambridge.org (L.K.B. Li).

¹ These authors contributed equally to this work.

¹ This is because the perturbation Mach number remains small even when the acoustic velocity fluctuation is large.

<http://dx.doi.org/10.1016/j.proci.2014.05.029>

1540-7489/© 2014 The Combustion Institute. Published by Elsevier Inc. All rights reserved.

Please cite this article in press as: S. Balusamy et al., *Proc. Combust. Inst.* (2014), <http://dx.doi.org/10.1016/j.proci.2014.05.029>

coustic system is therefore expected to behave like a coupled nonlinear dynamical system.

In a linear analysis, the flame response to perturbations at different frequencies is assumed to be the sum of the flame response at each of those frequencies. However, studies have shown that this is an oversimplification because significant energy can be transferred between frequencies, for example between a self-excited mode and a forced mode [2,3]. Crucially, in both simple and complex thermoacoustic systems [4,5], the oscillations are not necessarily periodic, but can be quasi-periodic, frequency-locked, chaotic, or synchronized with external forcing. Such systems can also exhibit mode switching as a result of the coexistence of two or more stable attractors. For a rigorous analysis, therefore, it is necessary to consider the system's response (i) in state space and/or (ii) at all frequencies, even when it is externally forced at only one.

In this paper, we take a dynamical systems approach to studying the nonlinear interaction between self-excited oscillations and forced oscillations in a combustor containing a swirl-stabilized turbulent premixed flame. Recent studies have shown that the forced response of hydrodynamically self-excited jets and flames at low Reynolds numbers can be explained by the forced response of simple (low-dimensional) model oscillators with weak nonlinearity [6–8]. Our aim is to see whether this also applies to a thermoacoustically self-excited system at a higher Reynolds number.

2. Experimental setup

Experiments are performed on an axisymmetric swirl-stabilized burner (Fig. 1). This burner has been used before to study the forced response of stratified flames [9] and the triggering of a premixed thermoacoustic system [10].

For this paper, a premixed flame is created by mixing air and methane, both metered with mass flow controllers (Alicat MCR series, $\pm 0.2\%$ FS). This reactant mixture is split into two streams: (i) one that enters a mixing plenum via a graduated bypass valve, and (ii) one that enters the same mixing plenum via a siren. The siren is used to generate acoustic velocity perturbations. It consists of a stator and a rotor, whose rotational speed determines the forcing frequency and is controlled by a variable-speed motor (EZ motor Model 55EZB500). The forcing amplitude is independently controlled by varying the opening of the graduated bypass valve.

The mixing plenum is 1000 mm long and consists of two concentric tubes (diameters: 15.05 and 27.75 mm) and an axisymmetric centerbody (diameter: 6.35 mm). The downstream ends of both tubes are aligned flush with the end of the

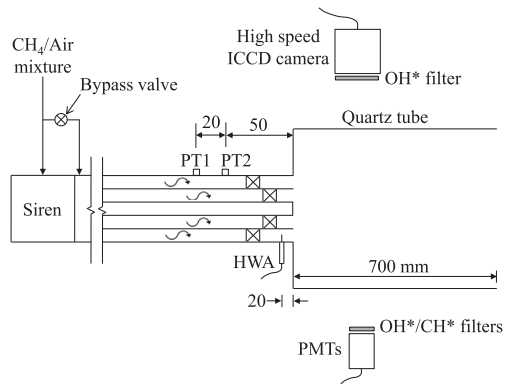


Fig. 1. Schematic of the swirl-stabilized turbulent premixed burner.

centerbody to form a well-defined burner exit. For flame stability, two axial swirlers are mounted in each annular section. Each swirler has six swirl vanes, of thickness 0.5 mm, aligned at 45° to the flow. For this geometry, the swirl number (i.e. the ratio of tangential to axial momentum) is estimated to be 0.55. Downstream of the burner exit is the combustor, which consists of a stainless steel dump plane and an optically accessible fused-silica tube with an inner diameter of 94 mm and a length of 700 mm. The exit of this tube is at ambient conditions. For certain flame conditions (Section 3.1), this combustor geometry supports thermoacoustically self-excited oscillations at the fundamental (longitudinal) mode of the tube.

These oscillations are examined by measuring the dynamic pressure in the mixing plenum with two pressure transducers (Model 40BP GRAS), one mounted 70 mm (PT1) and the other 50 mm (PT2) upstream of the dump plane. From these, the acoustic velocity fluctuation is calculated using the two-microphone technique [11] and the results are validated against hot-wire measurements taken 20 mm upstream of the dump plane in cold-flow conditions. The normalized pressure fluctuations from PT1 and PT2 are almost identical, so only the PT1 data will be used for characterizing the system's pressure response.

As an additional indicator, the global OH^* (308 ± 10 nm) and CH^* (430 ± 10 nm) chemiluminescence from the flame is measured using two photomultiplier tubes (Thorlabs model PMM01) fitted with bandpass filters. As is typical for premixed flames, the chemiluminescence emission is assumed to be proportional to the total heat-release rate. The normalized chemiluminescence intensities of OH^* and CH^* are almost identical, so only the OH^* data will be used for characterizing the system's heat-release response.

At each test point, the data are sampled at a frequency of 8192 Hz for 4 s on a data acquisition system (National Instruments, BNC-2111), resulting in a spectral resolution of 0.25 Hz and a

temporal resolution of 0.122 ms. All of the experiments are performed at ambient temperature and atmospheric pressure.

3. Results and discussion

3.1. Self-excited instability

Exploratory tests performed without forcing reveal several (unforced) operating conditions capable of supporting self-excited instability. This paper will focus on the one with the cleanest oscillations. This occurs at an equivalence ratio of 0.8, a bulk flow velocity of 10 m/s, a thermal input of 13.6 kW, and a Reynolds number of 8000.² The Reynolds number is based on the bulk flow velocity, the hydraulic diameter of the plenum tubes, and fluid properties at ambient conditions.

At this operating condition, the system exhibits self-excited limit-cycle oscillations at the fundamental mode of the combustor: $f_s = 195 \pm 3$ Hz. The normalized acoustic velocity at the burner exit is $u'/u = 6\% \pm 1.5\%$. The normalized pressure at PT1 is $p'/p = 0.1\% \pm 0.03\%$. The normalized heat-release at f_s is $q'/q = 4\% \pm 0.8\%$.

3.2. Forcing of the self-excited instability

The system is forced over a range of forcing frequencies, $20 \leq f_f \leq 400$ Hz, around the self-excited frequency, $f_s = 195$ Hz, in steps of 20 Hz.

At each f_f , the forcing amplitude, $A \equiv u'/u$, is increased from a minimum (Fig. 1: bypass valve fully opened) to a maximum (fully closed), and is then decreased from that maximum to a similar minimum. Figure 2 shows the specific values of these minima and maxima, along with their intermediate values. These are set by the interaction of the system with the siren, and are therefore dependent on f_f . The peak in A occurs at 200 Hz, which is near f_s , indicating that the forcing is amplified by the self-excited mode. Similar behavior has been seen in experiments on a realistic injector in pressurized conditions [3].

3.2.1. Overview at all forcing frequencies

For an overview of the nonlinear interaction between the self-excited and forced oscillations, we consider the power spectral density (PSD) of pressure and heat release. This is shown in Fig. 3 for the full range of f_f and for three different values of A (low, high, and low).

At low A (Fig. 3a and d: start of forcing), the self-excited mode appears as a vertical band of spectral peaks at $f_s = 195$ Hz. This mode coexists

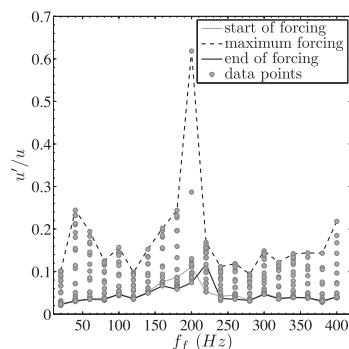


Fig. 2. Summary of the forcing amplitudes ($A \equiv u'/u$) and forcing frequencies (f_f) considered in this paper.

with the forced mode, which appears as a diagonal band at $f_f = f$ with a weak $f_f/8$ subharmonic. In Fig. 3d (heat release), two more diagonal bands corresponding to $|f_s \pm f_f|$ are also visible.

At high A (Fig. 3b and e: middle of forcing), the vertical band due to the self-excited mode is barely visible. In thermoacoustic systems involving combustion, the suppression of a self-excited mode by application of acoustic forcing at off-resonance frequencies has been reported only once before [2]. In contrast to this earlier study, we find that this suppression occurs strongly for both $f_f < f_s$ and $f_f > f_s$, and can lead to full synchronization (phase locking) for $f_f > f_s$ (Section 3.2.4).

When A is brought back to its initial low value (Fig. 3c and f: end of forcing), the self-excited mode reemerges but at 210 Hz, which is slightly higher than its initial value of 195 Hz. These final spectral peaks (at f_s) are also sharper and exhibit less scatter across the full range of f_f .

For the rest of this paper, we will focus on two specific forcing frequencies: one below f_s (Section 3.2.2) and one above f_s (Section 3.2.3).

3.2.2. Forced response when $f_f/f_s < 1$

Figure 4 shows the frequency spectrum of pressure at $f_f = 100$ Hz ($f_f/f_s = 0.51$) for both increasing A (Fig. 4a) and decreasing A (Fig. 4c).

When unforced ($A = 0$), the system has a self-excited mode at a natural frequency of $f_s = 195$ Hz (vertical dashed lines). When forced at a low amplitude ($A = 0.065$), the system responds at f_f as well as f_s , whose value, as noted earlier, shifts above its unforced value. This shifting occurs for a wide range of f_f : from 20 to 160 Hz. Because here $f_f/f_s < 1$, this shifting towards higher frequencies bears a resemblance to frequency pushing, a nonlinear phenomenon in which f_s is pushed away from f_f as A increases. Frequency pushing has been seen before in experiments [2] and simulations [12] on thermoacoustically self-excited combusting systems subjected to acoustic forcing. However, its physical origin in such systems has yet to be conclusively explained.

² This value of the Reynolds number is an order of magnitude higher than that in [6–8] but is an order of magnitude lower than that in actual gas turbines.

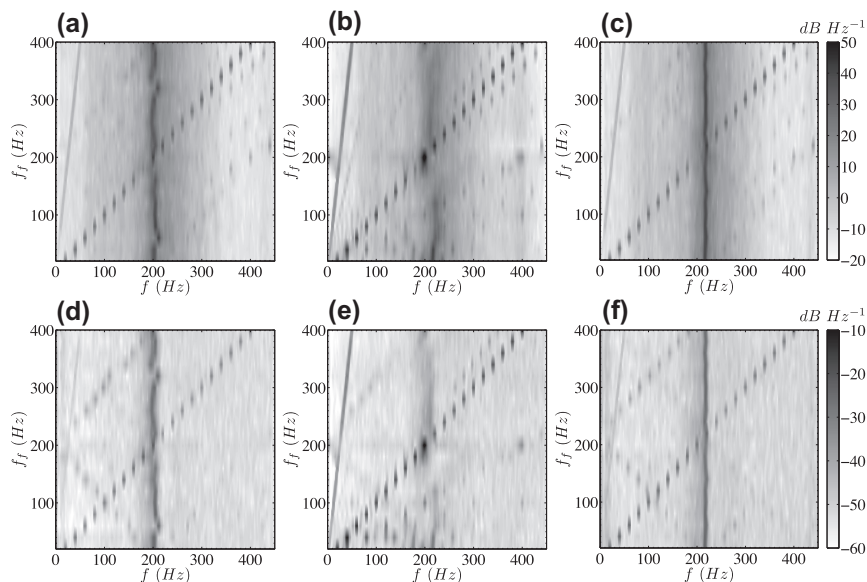


Fig. 3. PSD of pressure fluctuations (top row) and heat-release fluctuations (bottom row) at the start (left), middle (center), and end (right) of the forcing program. From left to right, the forcing amplitude goes from low, maximum, and then back to low as per Fig. 2.

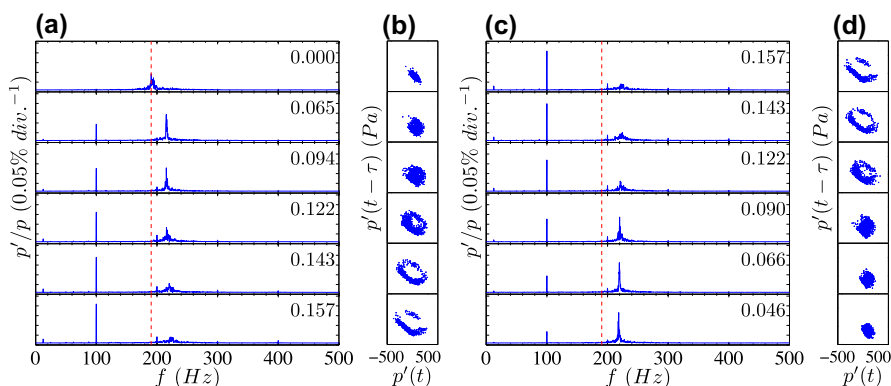


Fig. 4. Spectra (a and c) and Poincaré map (b and d) of pressure at a forcing frequency of 100 Hz ($f_f/f_s = 0.51$) for various forcing amplitudes ($A \equiv u'/u$, indicated in plot). The forcing amplitude is first increased from a minimum to a maximum (a and b), and then it is decreased from that maximum to a similar minimum (c and d). The vertical dashed lines indicate the unforced self-excited frequency.

Nevertheless, in magnetrons, it has been attributed to strongly nonlinear electron-wave interactions that change the mean field [13]. We speculate that an analogous effect, acting on the mean flow field and/or the mean temperature field, may be responsible for frequency pushing in thermoacoustic systems such as this one. To test this hypothesis, we would need to perform detailed measurements of the velocity field and the temperature field, which is beyond the scope of this paper. Regardless of its physical mechanism, frequency pushing seems to be a common feature of nonlinear dynamical systems. This is

supported by the fact that it can be modeled easily by including a Duffing (cubic restoring force) term in the van der Pol oscillator [14,15].

As A increases, the self-excited mode weakens until it nearly disappears at maximum A (0.157). Then, as A decreases, it reemerges and grows until the end of forcing. In this latter stage, the self-excited frequency shifts to a slightly lower value but does not return to the initial 195 Hz, while the self-excited amplitude grows above its initial value, indicating hysteresis.

The dynamics of this system can be understood more easily by inspecting the topology of its

reconstructed state space via the (one-sided) Poincaré map.³ This is shown in Fig. 4(b and d). The time delay used in the reconstruction, τ , controls the degree to which the attractor is unfolded in its embedding space. For this paper, the optimal value⁴ of τ is found using the first zero-crossing of the autocorrelation function of p' .

When $A = 0$, the trajectory in state space is closed because the self-excited system oscillates periodically in a limit cycle (at f_s). In the Poincaré map, the data points are therefore clustered around one blob. If the system were free of noise, the trajectory would be perfectly closed and the Poincaré map would show one discrete point. (This interpretation of the dynamics is consistent with the frequency spectrum, which shows a single peak.) As A increases, the trajectory in state space starts to spiral around the surface of a torus. In the Poincaré map, this is seen as a ring (first visible at $A = 0.122$). The appearance of a torus attractor is characteristic of quasiperiodicity. In this system, because there are two dominant, but incommensurate, frequencies (f_f and f_s), the oscillations are said to be two-frequency quasiperiodic. The ring in the Poincaré map grows as A increases, but then shrinks as A decreases from its maximum ($A = 0.157$). Eventually, the ring closes ($A = 0.090$), indicating a return to periodicity. This sequence of bifurcations occurs for a wide range of f_f , although, as will be discussed in Section 3.2.3, it is not always clear owing to noise.

In the dynamical systems framework, the system is said to have undergone two bifurcations: (i) as A increases, the system transitions from periodicity to two-frequency quasiperiodicity via a torus-birth (Neimark–Sacker) bifurcation; then (ii) as A decreases, the system transitions from two-frequency quasiperiodicity to periodicity via a torus-death (inverse Neimark–Sacker) bifurcation. Similar behavior was recently seen in experiments on forced hydrodynamically self-excited jets and flames at low Reynolds numbers [6–8]. Crucially, this behavior is also seen in the forced response of simple (low-dimensional) model oscillators, such as the van der Pol oscillator [14,17]. This similarity in the nonlinear dynamics of disparate systems suggests that, with further analysis, it may be possible to represent thermoacoustically self-excited systems, such as this one, using simple model oscillators.

³ The Poincaré map is a two-dimensional slice through the three-dimensional state space, which, for this paper, is reconstructed with time-delay embedding (please see [16] for a review of nonlinear time-series analysis).

⁴ The optimal value of τ varies only slightly with A . In Figs. 4 and 5, it is held constant for a given f_f in order to aid comparison across different values of A .

3.2.3. Forced response when $f_f/f_s > 1$

Figure 5 is analogous to Fig. 4 ($f_f/f_s = 0.51$) but for $f_f = 300$ Hz ($f_f/f_s = 1.54$). For both values of f_f , the self-excited amplitude decreases as A increases, but reemerges as A decreases. Moreover, f_s always shifts above its initial value (195 Hz) at the end of forcing. For $f_f/f_s = 0.51$ (Section 3.2.2), this was interpreted as frequency pushing. Here, for $f_f/f_s = 1.54$, it is interpreted as frequency pulling, which, like frequency pushing, is a common feature of nonlinear dynamical systems and can be modeled with universal model oscillators [18].

There are also subtle differences between forcing above f_s and below f_s . For $f_f/f_s = 1.54$ (Fig. 5b and d), the Poincaré map shows data points whose scatter (i) increases initially with A but then (ii) decreases to a minimum at maximum A (0.149). We interpret this as follows:

- (i) As A initially increases, the system undergoes a torus-birth bifurcation from periodicity to two-frequency quasiperiodicity, much as it did in Section 3.2.2. The absence of a clear ring in the Poincaré map could be due to excessive noise in the system, which blurs the state-space trajectory such that it does not spiral perfectly around the torus attractor.
- (ii) Once A becomes sufficiently large, the system synchronizes with the forcing, causing its oscillations to become periodic and its (noisy) state-space trajectory to collapse onto a closed loop. In the Poincaré map, this should lead to a reduction in the data scatter, which is indeed what is observed at $A = 0.114 \rightarrow 0.149$. Given that the self-excited amplitude (at f_s) decreases gradually (not abruptly) with A , we speculate that this transition from two-frequency quasiperiodicity to periodicity occurs via a torus-death bifurcation [18].

As A eventually decreases ($0.149 \rightarrow 0.047$), the above sequence of transitions and bifurcations recurs in reverse order. As noted in Section 3.2.2, all of these nonlinear dynamics can be found in the forced response of universal model oscillators, such as the forced van der Pol oscillator [14,17].

3.2.4. Phase dynamics of synchronization

In universal model oscillators, synchronization can occur partially (phase trapping) or fully (phase locking).⁵ In this section, we examine the degree to which synchronization occurs in the system. We use the Hilbert transform to compute the

⁵ For an explanation of these terms, please see specialized texts [17,18] and recent papers on the subject [8,19].

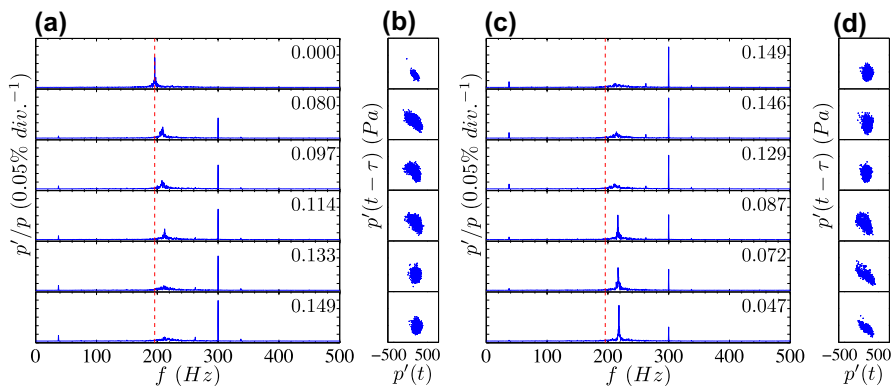


Fig. 5. Spectra (a and c) and Poincaré map (b and d) of pressure at a forcing frequency of 300 Hz ($f_f/f_s = 1.54$) for various forcing amplitudes ($A \equiv u'/u$, indicated in plot). The forcing amplitude is first increased from a minimum to a maximum (a and b), and then it is decreased from that maximum to a similar minimum (c and d). The vertical dashed lines indicate the unforced self-excited frequency.

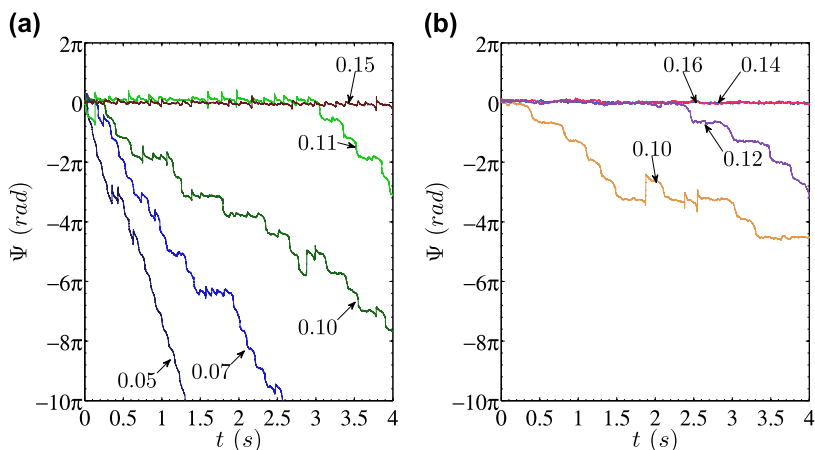


Fig. 6. Phase difference $\Psi(t)$ at a forcing frequency of $f_f = 220$ Hz ($f_f/f_s = 1.13$) for increasing (a) and decreasing (b) forcing amplitudes ($A \equiv u'/u$, indicated in plot). For each A , $\Psi(t = 0)$ is reset to zero in order to aid comparison of its temporal evolution.

instantaneous phase of p' at PT1: $\psi_s(t)$. By applying the same transform to the forcing signal (siren input), we obtain its instantaneous phase, $\psi_f(t)$, which we subtract from $\psi_s(t)$ to get the phase difference: $\Psi(t) \equiv \psi_s(t) - \psi_f(t)$. This is a suitable indicator of the phase dynamics [17].

Figure 6 shows $\Psi(t)$ at $f_f = 220$ Hz ($f_f/f_s = 1.13$) for both increasing A (Fig. 6a) and decreasing A (Fig. 6b). At low A (0.05), the system responds by phase drifting: $\Psi(t)$ decreases unboundedly with time, with occasional phase slips. As A increases (0.05 \rightarrow 0.10), the time-averaged slope of $\Psi(t)$ is pulled towards zero, indicating that the time-averaged frequency of the system is pulled towards that of the forcing. This concurs with the frequency pulling seen in Section 3.2.3. Within a higher range of A (0.11–0.15), the system

responds by phase trapping: $\Psi(t)$ oscillates periodically but remains bounded such that its time-averaged slope is exactly zero, indicating frequency locking without phase locking [17]. On initial entry into this partially synchronous state ($A = 0.11$), the system remains stable for only a limited period of time (~ 2.7 s), after which it switches to a state of phase drifting.

At maximum A (0.16; Fig. 6b), the system responds by phase locking: $\Psi(t)$ becomes constant with time, indicating that the system spends all of its time oscillating at f_f , i.e. it is fully synchronized with the forcing. In this system, phase drifting and phase slipping occur for both $f_f > f_s$ and $f_f < f_s$, but phase locking occurs only for $f_f > f_s$. As A decreases from its maximum, the system transitions directly from phase locking ($A = 0.16$ –0.14)

to phase drifting ($A = 0.12$) without undergoing phase trapping, which is in contrast to its behavior for increasing A (Fig. 6a). This indicates hysteresis, which could be due to a narrowing of the A range within which phase trapping occurs. Hysteresis can also be seen in the difference in the time-averaged slope of $\Psi(t)$ at $A = 0.10$ between increasing A (Fig. 6a) and decreasing A (Fig. 6b).

All four types of behavior (phase drifting, slipping, trapping, and locking) have been observed in forced hydrodynamically self-excited jets [8] and in forced model oscillators. In the latter case, it can be studied analytically and therefore understood. This shows that these types of behavior are not limited to this particular system, but are general features of forced nonlinear oscillators.

4. Conclusions

We have presented experimental evidence for a range of nonlinear dynamics from an acoustically forced thermoacoustically self-excited combustor system: a swirl-stabilized turbulent lean-premixed flame in a tube driven by a siren.

Some of these dynamics have not, to our knowledge, been observed in such a system before. They include (i) a shifting of the self-excited frequency towards or away from the forcing frequency as the forcing amplitude increases (seen in spectra); (ii) an accompanying transition from periodicity to two-frequency quasiperiodicity (seen in the Poincaré map); (iii) an eventual suppression of the self-excited amplitude for forcing frequencies both above and below the self-excited frequency (seen in spectra); and (iv) phase trapping (seen via the Hilbert transform).

All of these dynamics can be found in universal model oscillators subjected to external forcing [17]. This suggests that such oscillators can be used to accurately represent thermoacoustically self-excited combustor systems subjected to similar forcing. It also suggests that the analytical solutions to such oscillators can be used (i) to gain new insight into the physical mechanisms behind thermoacoustic instability; (ii) to develop new strategies for passively or actively controlling thermoacoustic instability, e.g. as a testbed for novel control algorithms; (iii) to investigate how thermoacoustic oscillations in the combustor interact with flow oscillations in other sub-systems, such as plenums and Helmholtz resonators; (iv) to examine the effect of different types of noise on the system's stability; and (v) to guide the reduction and analysis of experimental or numerical data obtained from real thermoacoustic systems, thus helping to identify subtle behavior that would perhaps otherwise be overlooked.

One of the open questions in thermoacoustics is how the presence of a hydrodynamically self-excited flame (whose heat-release rate oscillates

at a natural hydrodynamic frequency [20]) affects the onset, development and saturation of thermoacoustic oscillations at nearby acoustic frequencies. In this paper, we cannot address this question directly because the flame is not hydrodynamically self-excited. Nevertheless, we can address it indirectly by noting that there are strong similarities between the two cases, even if the physical mechanism of self-excitation is different.⁶ Both cases involve a self-excited mode interacting with a forced mode over a wide range of forcing amplitudes – from low amplitudes, where only limited nonlinear interaction between the two modes occurs, to high amplitudes, where full synchronization occurs. Hence, given that many of the qualitative features of low-order dynamical systems are universal [21], the current findings should also be applicable to the case in which a hydrodynamically self-excited flame interacts with the combustor acoustics to produce coupled thermoacoustic oscillations.

Finally, the ability to weaken a self-excited mode with external forcing in this model combustor has potential implications for the existing concept of using open-loop control to weaken thermoacoustic modes in industrial combustors, such as those in gas turbines. Further work under increasingly realistic conditions should reveal the extent to which the current findings carry over into industrial systems.

Acknowledgments

This work was funded by EPSRC-UK under the SAMULET Project (EP/G035784/1). The technical assistance of Roy Slater is gratefully acknowledged.

References

- [1] T.C. Lieuwen, V. Yang, F.K. Lu (Eds.), *Combustion instabilities in gas turbine engines: operational experience, fundamental mechanisms and modeling*, American Institute of Aeronautics and Astronautics, 2005.
- [2] B. Bellows, A. Hreiz, T. Lieuwen, *J. Propul. Power* 24 (2008) 628–631.

⁶ In the case of a hydrodynamically self-excited flame, the self-excited mode arises from the hydrodynamics of the flame, and the forced mode arises from the (self-excited) thermoacoustics of the coupled flame-acoustic system. In the case considered in this paper, the self-excited mode arises from the thermoacoustics of the coupled flame-acoustic system (the flame itself is not self-excited in any way), and the forced mode arises from externally applied acoustic oscillations.

- [3] S. Hochgreb, D. Dennis, I. Ayranci, W. Bainbridge, S. Cant, in: *Proceedings of the ASME Turbo Expo*, 2013, GT2013-9531.
- [4] L. Kabiraj, R. Sujith, P. Wahi, *J. Eng. Gas Turb. Power* 134 (2012) 031502.
- [5] H. Gotoda, H. Nikimoto, T. Miyano, S. Tachibana, *Chaos* 21 (2011) 013124.
- [6] L.K.B. Li, M.P. Juniper, *Proc. Combust. Inst.* 34 (2013) 947–954.
- [7] L.K.B. Li, M.P. Juniper, *J. Fluid Mech.* 726 (2013) 624–655.
- [8] L.K.B. Li, M.P. Juniper, *J. Fluid Mech.* 735 (2013) R5.
- [9] K. Kim, S. Hochgreb, *Combust. Flame* 158 (2011) 2482–2499.
- [10] K.T. Kim, S. Hochgreb, *Combust. Flame* 159 (2012) 1215–1227.
- [11] A.F. Seybert, D.F. Ross, *J. Acoust. Soc. Am.* 61 (1977) 1362–1370.
- [12] K. Kashinath, Nonlinear Thermoacoustic Oscillations of a Ducted Premixed Flame, PhD thesis, University of Cambridge, Department of Engineering, United Kingdom, 2013.
- [13] S. Chen, *IEEE T. Plasma Sci.* 18 (1990) 570–576.
- [14] B. vander Pol, J. vander Mark, *Nature* 120 (1927) 363–364.
- [15] J. Walsh, G. Johnston, R. Davidson, D. Sullivan, in: OE/LASE'89, International Society for Optics and Photonics, Los Angeles, CA, 1989, pp. 161–169.
- [16] H. Kantz, T. Schreiber, *Nonlinear Time Series Analysis*, 2nd ed., Cambridge University Press, Cambridge, England, 2003.
- [17] A. Pikovsky, M. Rosenblum, J. Kurths, *Synchronization: A Universal Concept in Nonlinear Sciences*, 12, Cambridge university press, 2003.
- [18] A. Balanov, N. Janson, D. Postnov, O. Sosnovtseva, in: *Synchronization: From Simple to Complex*, Springer Series in Synergetics, Springer-Verlag, Heidelberg, Germany, 2009.
- [19] J. Thévenin, M. Romanelli, M. Vallet, M. Brunel, T. Erneux, *Phys. Rev. Lett.* 107 (2011) 104101.
- [20] M. Juniper, L. Li, J. Nichols, *P. Combust. Inst.* 32 (2009) 1191–1198.
- [21] P. Manneville, *Instabilities, Chaos and Turbulence*, 2nd ed., Imperial College Press., London, England, 2010.